INSTITUTE OF PHYSICS PUBLISHING JOURNAL OF PHYSICS D: APPLIED PHYSICS

J. Phys. D: Appl. Phys. **34** (2001) 574–583 www.iop.org/Journals/jd PII: S0022-3727(01)18279-3

Effect of multiple pulses on the plasma chemistry during the remediation of NO_x using dielectric barrier discharges

Rajesh Dorai[1] **and Mark J Kushner**[2,3]

[1] Department of Chemical Engineering, University of Illinois, 1406 W Green St, Urbana, IL 61801, USA

[2] Department of Electrical and Computer Engineering, University of Illinois, 1406 W Green St, Urbana, IL 61801, USA

E-mail: dorai@uiuc.edu and mjk@uiuc.edu

Received 24 October 2000

Abstract

Dielectric barrier discharges (DBDs) are being investigated to remediate NO_x from atmospheric gas streams. The interaction of species generated during previous pulses of repetitively pulsed devices, such as DBDs, make their operation fundamentally different from single pulse operation. To investigate these effects, the reaction chemistry of multiple pulses during NO_x remediation was modelled. Reactions between radicals produced during a pulse with the products from previous pulses produce significantly different end products. For example, approximately 10 ppm of methyl nitrate (CH_3ONO_2) was obtained by multiple pulsing whereas less than 1 ppm of it was produced with single discharge formats. Multiple pulsing has also been found to be more efficient for NO_x remediation. W-values for NO_x remediation decreased from 240 eV for a single pulse (58 J l^{-1}) to 185 eV when the same energy was distributed over 20 pulses.

1. Introduction

Plasma remediation is being investigated to remove NO_x (oxides of nitrogen) from atmospheric gas streams [1–18]. A variety of plasma reactors have been studied for NO_x remediation, including, e-beam [1–8], pulsed corona discharges [9–15] and dielectric barrier discharges (DBDs) [9, 10, 16–21]. In the case of DBDs and pulsed corona discharges, each volume of gas is typically processed by many short discharge pulses (≈100 s of ns duration). During each discharge pulse, electron impact reactions produce radicals which initiate chemical reactions. Typical exhausts contain N_2, O_2, H_2O and CO_2 (mostly from the unreacted excess air and combustion products) with ppm levels of NO_x (primarily NO), CO, H_2 and unburned hydrocarbons (UHCs) due to the incomplete combustion of the fuel. Plasma processing of NO_x is dominantly oxidative due to the presence of H_2O and O_2 [16, 22–24], resulting primarily in NO_2, and to some extent in HNO_3, HNO_2. The desired process is the reduction of NO_x to N_2.

Simple hydrocarbons have been studied in simulated exhausts to investigate the effects of UHCs. For example, Niessen *et al* [16] examined ethene (C_2H_4) as an additive to a NO_x–humid air mixture. Penetrante *et al* [22] investigated the consequences of propene (C_3H_6) in a NO_x-air feed. Both studies showed that UHCs significantly contribute to NO oxidation. Niessen *et al* [16] found that adding 2000 ppmv C_2H_4 improved the NO removal efficiency from 60 to 5–10 eV with most of the remediated NO being converted to NO_2. With propene addition, Penetrante *et al* [22] found that, at 300 °C, almost 100% of the initial NO (500 ppm) was converted to NO_2 whereas in the absence of propene, only 7% of NO was remediated.

Since the plasma largely converts NO to NO_2 in the presence of UHCs, attempts have been made to couple the process with catalytic converters to promote reduction of the NO_2 to N_2 [22, 23]. Penetrante *et al* [22] observed as high as 55% NO_x conversion to N_2 at 370 °C using pulsed corona reactors packed with γ-Al_2O_3 pellets. Balmer *et al* [23] showed that the use of alumina and Na-ZSM-5 catalysts with plasma reactors produced 40 and 50% NO_x reduction, but the processes were energy intensive.

Industrial systems for plasma processing of toxic gases typically operate at sufficiently high repetition rates that a given sample of gas is subjected to several discharge pulses. Pulses

[3] Author to whom correspondence should be addressed.

with short rise-time and high amplitude voltage have been found to be advantageous due to their ability to rapidly produce high E/N (electric field/number density) [25]. It has also been found that it is more efficient with respect to remediation to deposit a given amount of energy in a large number of shorter duration pulses [19]. With each pulse, radicals initiating the plasma chemistry are generated and during the inter-pulse period, these radicals undergo reactions thereby changing the composition of the plasma. The reaction chemistry for the follow-on pulses is different from that which would be obtained from an equivalent energy deposition in a single or smaller number of pulses due to the accumulation of these inter-pulse products.

In this paper, we discuss the consequences of inter-pulse chemistry on the plasma remediation of NO_x in a DBD reactor. We found that with multiple pulses, approximately 10 ppm of methyl nitrate (CH_3ONO_2) and 16 ppm of ethyl nitrate ($C_2H_5ONO_2$) was formed, whereas less than 1 ppm of each were produced with a single pulse. The efficiency of NO_x remediation improved from 240 eV per molecule for a single pulse to 185 eV per molecule when the same energy (58 J L^{-1}) was distributed over 20 pulses. The model used for this study, GLOBAL_KIN, is described in section 2. The reaction mechanism for the NO_x–propene–propane mixture is summarized in section 3. NO_x processing with multiple pulse formats is discussed in section 4. Concluding remarks are given in section 5.

2. Description of the model

The model used in our investigation is called GLOBAL_KIN and is described in detail in [26]. GLOBAL_KIN is a spatially homogenous model and consists of three main modules: a plasma chemistry module, a circuit module and a Boltzmann equation module. From the user-defined reaction mechanism, the plasma chemistry module constructs differential equations for the evolution of species and the electron temperature, and the circuit module provides the E/N in the plasma. To obtain the electron impact reaction rate coefficients, Boltzmann's equation is solved offline for the electron energy distribution to generate a table of reaction rate coefficients as a function of E/N or equivalently electron temperature. The final set of ordinary differential equations is then integrated in time using LSODE [27], a stiff equation solver. The time steps chosen for integration are dynamically adjusted to capture the dynamics of the system at any particular time and spans greater than 10^9 orders of magnitude. In order to capture the features of multiple discharges, the model is run for a series of current pulses and afterglow time periods. The total number of pulses is divided equally over the residence time used for the single-pulse case. The energy deposition is varied by either changing the applied voltage, the dielectric thickness or the dielectric permittivity.

The residence time of the gas was 0.2 s and the reactor was operated at 453 K (180 °C) and 1 atm. The gas gap was 2.5 mm and the energy deposition for the base case was 30 J L^{-1}. The repetition rate was 100 Hz (20 pulses distributed equally over 0.2 s).

3. Reaction mechanism

The reaction mechanism for NO_x remediation can be described by two trees: reactions with and without UHCs. The detailed mechanism for NO_x in the absence of UHCs is described in [19]. In summary, in the absence of UHCs, NO_x is remediated primarily by two channels:

Reduction:

$$\mathrm{NO + N \rightarrow N_2 + O}$$
$$k = 3.41 \times 10^{-11} \exp(-24/T)\ \mathrm{cm^3\ s^{-1}},$$
$$k_{298} = 3.2 \times 10^{-11}\ \mathrm{cm^3\ s^{-1}}. \quad (1)$$

Oxidation:

$$\mathrm{NO + O_3 \rightarrow NO_2 + O_2}$$
$$k = 4.3 \times 10^{-12} \exp(-1598/T)\ \mathrm{cm^3\ s^{-1}},$$
$$k_{298} = 2.1 \times 10^{-14}\ \mathrm{cm^3\ s^{-1}} \quad (2a)$$
$$\mathrm{NO + O + M \rightarrow NO_2 + M}$$
$$k = 6.71 \times 10^{-32} (T/298)^{-1.41}\ \mathrm{cm^6\ s^{-1}} \quad (2b)$$
$$\mathrm{NO + HO_2 \rightarrow NO_2 + OH}$$
$$k = 3.5 \times 10^{-12} \exp(240/T)\ \mathrm{cm^3\ s^{-1}},$$
$$k_{298} = 7.8 \times 10^{-12}\ \mathrm{cm^3\ s^{-1}} \quad (2c)$$
$$\mathrm{NO + OH + M \rightarrow HNO_2 + M}$$
$$k = 8.64 \times 10^{-31} (T/298)^{-2.51} \exp(34/T)\ \mathrm{cm^6\ s^{-1}},$$
$$k_{298} = 9.7 \times 10^{-31}\ \mathrm{cm^6\ s^{-1}} \quad (2d)$$

$$\mathrm{NO_2 + OH + M \rightarrow HNO_3 + M}$$
$$k = 4.62 \times 10^{-29} (T/298)^{-5.49} \exp(-1183/T)\ \mathrm{cm^6\ s^{-1}},$$
$$k_{298} = 8.7 \times 10^{-31}\ \mathrm{cm^6\ s^{-1}}. \quad (3)$$

k is the rate coefficient and k_{298} is its value at $T = 298$ K. O, N and OH are produced by electron impact reactions with O_2, N_2 and H_2O, respectively.

$$\mathrm{e + O_2 \rightarrow O + O + e} \quad (4)$$

$$\mathrm{e + N_2 \rightarrow N + N + e} \quad (5)$$

$$\mathrm{e + H_2O \rightarrow OH + H + e.} \quad (6)$$

O_3 is produced by the reaction of O with O_2,

$$\mathrm{O + O_2 + M \rightarrow O_3 + M}$$
$$k = 3.4 \times 10^{-34} (T/298)^{-1.2}\ \mathrm{cm^6\ s^{-1}}. \quad (7)$$

HO_2 is produced by the reaction of H with O_2,

$$\mathrm{H + O_2 + M \rightarrow HO_2 + M}$$
$$k = 1.78 \times 10^{-32} (T/298)^{-0.8}\ \mathrm{cm^6\ s^{-1}}. \quad (8)$$

H by itself is formed by the electron impact dissociation of H_2O (equation (6)) and by the reaction of O with OH,

$$\mathrm{O + OH \rightarrow O_2 + H}$$
$$k = 4.55 \times 10^{-12} (T/298)^{0.4} \exp(372/T)\ \mathrm{cm^3\ s^{-1}},$$
$$k_{298} = 1.6 \times 10^{-11}\ \mathrm{cm^3\ s^{-1}}. \quad (9)$$

In the absence of UHCs, the consumption of NO_x mainly occurs through the oxidation channel. This is due to the fact that the rates of producing O and OH are higher compared to N because of the lower dissociation energy of H_2O and O_2 compared to N_2.

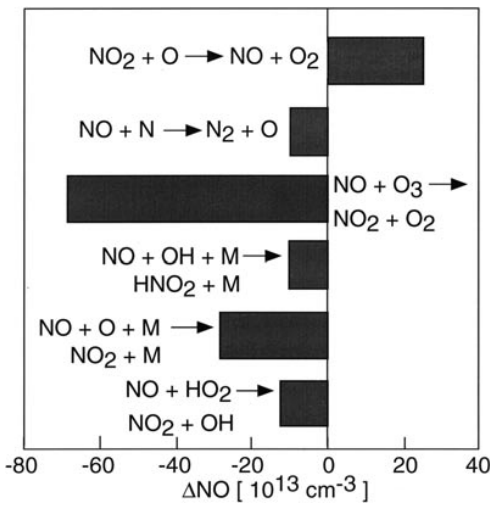

Figure 1. Individual contributions of various reaction channels towards the remediation of NO during the DBD processing of NO_x in the absence of UHCs. The base gas mixture contains $N_2/O_2/H_2O/CO_2 = 79/8/6/8$ with 260 ppm of NO, 400 ppm of CO and 133 ppm of H_2. The energy deposition is 30 J L^{-1}. The reactor temperature and pressure are 453 K and 1 atm. In the absence of UHCs, the dominant reaction channels result in the oxidation of NO to NO_2. The reduction channel, $NO + N \rightarrow N_2 + O$, accounts for only 8% of the NO remediation.

For example, the contributions of each of the above channels to NO remediation in a mixture with 8% O_2, 6% H_2O, 7% CO_2, 400 ppm CO, 260 ppm NO, 133 ppm H_2 and balance N_2 are given in figure 1. At 30 J L^{-1}, the reduction channel (equation (1)) accounts for only 8% of the total NO remediation. Oxidation by O_3 is the dominant consumption pathway for NO (equation (2*a*)).

The reaction mechanism for NO_x in the presence of propane (C_3H_8) and propene (C_3H_6) is discussed in detail in [26] and is summarized in figure 2. In the presence of the UHCs, C_3H_6 and C_3H_8, new pathways for NO oxidation are introduced, most of which primarily result in the formation of NO_2. The reactivity of propane, is smaller compared to propene, as approximately only 5% propane is consumed at the end of a typical process [40 J L^{-1}] compared to 50% for propene. Briefly, the initiating processes for the C_3H_6 and C_3H_8 chains are reactions with O and OH:

$$OH + H_3C{-}CH{=}CH_2 \rightarrow (0.35)\ H_3C{-}CH(OH){-}CH_2$$
$$+(0.65)\ H_3C{-}CH{-}CH_2OH$$
$$k = 4.85 \times 10^{-12} \exp(504/T)\ \text{cm}^3\ \text{s}^{-1},$$
$$k_{298} = 2.6 \times 10^{11}\ \text{cm}^3\ \text{s}^{-1} \qquad (10)$$

$$O + H_3C{-}CH{=}CH_2 \rightarrow CH_3{-}\overset{O}{\overset{/\quad\backslash}{CH}}{-}CH_2 \quad (30\%) \qquad (11)$$
$$\rightarrow CH_3CH_2CHO \quad (30\%) \qquad (12)$$
$$\rightarrow CH_2CHO + CH_3 \quad (20\%) \qquad (13)$$
$$\rightarrow HCO + C_2H_5 \quad (20\%) \qquad (14)$$
$$k = 4 \times 10^{-12}\ \text{cm}^3\ \text{s}^{-1}$$

$$OH + H_3C{-}CH_2CH_3 \rightarrow H_3C{-}CH_2{-}CH_2 + H_2O$$
$$k = 7.95 \times 10^{-13}(T/298)^2 \exp(-227/T)\ \text{cm}^3\ \text{s}^{-1},$$
$$k_{298} = 3.7 \times 10^{-13}\ \text{cm}^3\ \text{s}^{-1} \qquad (15)$$

$$\rightarrow H_3C{-}CH{-}CH_3 + H_2O$$
$$k = 1.44 \times 10^{-12}(T/298) \exp(130/T)\ \text{cm}^3\ \text{s}^{-1},$$
$$k_{298} = 2.2 \times 10^{-12}\ \text{cm}^3\ \text{s}^{-1}. \qquad (16)$$

The hydroxyalkyl and alkyl radicals formed by the reactions in equations (10), (15) and (16) then quickly react with O_2 to form the peroxy radicals,

$$H_3C{-}CH(OH){-}CH_2 + O_2 \rightarrow H_3C{-}CH(OH){-}CH_2OO$$
$$k = 3.82 \times 10^{-12}\ \text{cm}^3\ \text{s}^{-1} \qquad (17)$$
$$H_3C{-}CH{-}CH_2OH + O_2 \rightarrow H_3C{-}CH(OO){-}CH_2OH$$
$$k = 1.16 \times 10^{-11}\ \text{cm}^3\ \text{s}^{-1} \qquad (18)$$
$$H_3C{-}CH_2{-}CH_2 + O_2 \rightarrow H_3C{-}CH_2{-}CH_2OO$$
$$k = 8 \times 10^{-12}\ \text{cm}^3\ \text{s}^{-1} \qquad (19)$$
$$H_3C{-}CH{-}CH_3 + O_2 \rightarrow H_3C{-}CH(OO){-}CH_3$$
$$k = 1.1 \times 10^{-11}\ \text{cm}^3\ \text{s}^{-1}. \qquad (20)$$

These peroxy radicals (R–OO) then react with NO to convert it into NO_2,

$$R{-}OO + NO \rightarrow R{-}O + NO_2 \qquad (21)$$

where R is the alkyl or hydroxyalkyl part of the peroxy radical.

Some amount of NO remediation is also achieved through the formation of organic nitrates and nitrites. For example, CH_3O, formed from a two-step reaction beginning with CH_3, reacts with NO to form CH_3ONO (methyl nitrite).

$$CH_3 + O_2 + M \rightarrow CH_3O_2 + M$$
$$k = 4.41 \times 10^{-31}(T/298)^{-3}\ \text{cm}^6\ \text{s}^{-1} \qquad (22)$$
$$CH_3O_2 + NO \rightarrow CH_3O + NO_2$$
$$k = 4.2 \times 10^{-12} \exp(180/T)\ \text{cm}^3\ \text{s}^{-1},$$
$$k_{298} = 7.7 \times 10^{-12}\ \text{cm}^3\ \text{s}^{-1} \qquad (23)$$
$$CH_3O + NO \rightarrow CH_3ONO$$
$$k = 2.0 \times 10^{-11}\ \text{cm}^3\ \text{s}^{-1}. \qquad (24)$$

CH_3 is primarily produced by the reaction in equation (13). CH_3O also reacts with NO_2 to form CH_3ONO_2 (methyl nitrate):

$$CH_3O + NO_2 \rightarrow CH_3ONO_2 \qquad k = 8.32 \times 10^{-12}\ \text{cm}^3\ \text{s}^{-1}. \qquad (25)$$

Similar chemistry is observed when C_2H_5O, formed from C_2H_5, reacts with NO to generate C_2H_5ONO (ethyl nitrite),

$$C_2H_5 + O_2 + M \rightarrow C_2H_5O_2 + M$$
$$k = 8.02 \times 10^{-26}(T/298)^{-8.24} \exp(-2150/T)\ \text{cm}^6\ \text{s}^{-1},$$
$$k_{298} = 5.0 \times 10^{-29}\ \text{cm}^6\ \text{s}^{-1} \qquad (26)$$
$$C_2H_5O_2 + NO \rightarrow C_2H_5O + NO_2$$
$$k = 3.1 \times 10^{-12} \exp(330/T)\ \text{cm}^3\ \text{s}^{-1},$$
$$k_{298} = 9.4 \times 10^{-12}\ \text{cm}^3\ \text{s}^{-1} \qquad (27)$$
$$C_2H_5O + NO \rightarrow C_2H_5ONO$$
$$k = 2.0 \times 10^{-11}\ \text{cm}^3\ \text{s}^{-1}. \qquad (28)$$

C_2H_5 is produced by the reaction of O with C_3H_6 (equation (14)). C_2H_5O also reacts with NO_2 to form $C_2H_5ONO_2$ (ethyl nitrate).

$$C_2H_5O + NO_2 \rightarrow C_2H_5ONO_2 \qquad k = 1.32 \times 10^{-11}\ \text{cm}^3\ \text{s}^{-1}. \qquad (29)$$

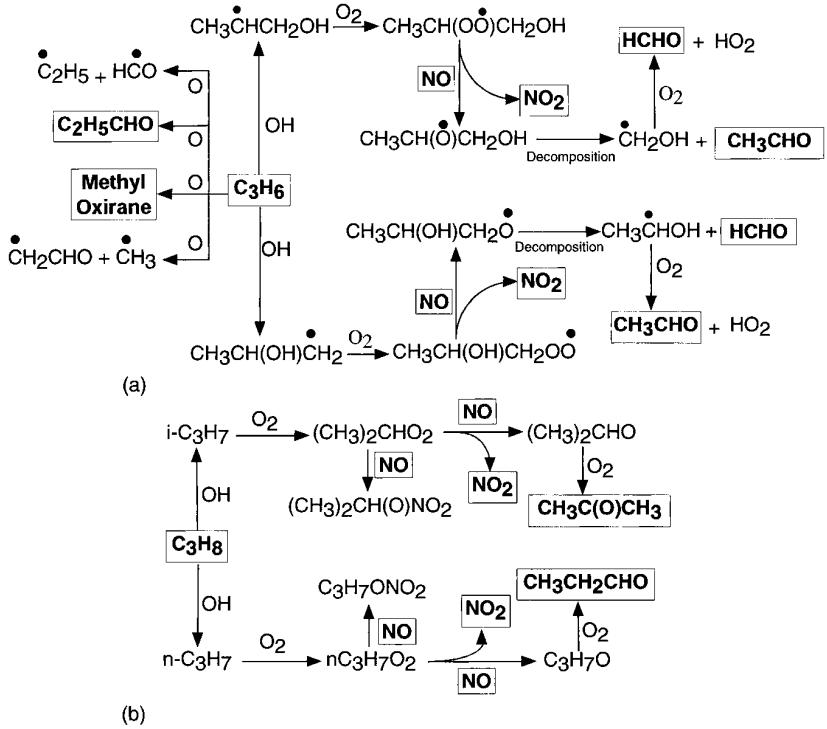

Figure 2. Reaction mechanism for NO_x in the presence of C_3H_8 and C_3H_6.

4. Plasma processing of NO_x in the presence of UHCs using single- and multiple-pulse formats

To validate the model, comparisons were made of computed results to experiments conducted by Khacef *et al* [28] for DBD processing of NO in the presence of hydrocarbons. The 1 atm, 530 K gas feed contained 500 ppm NO, 500 ppm C_3H_6, 10% O_2 and 10% H_2O, with the balance being N_2. The reactor was a cylindrical wire-to-cylinder apparatus with a 0.5 cm gap. Comparison conditions were a repetition rate of 100 Hz and residence time of 0.1 s. Exit NO and NO_2 densities as a function of energy deposition are shown in figure 3(a). With increasing energy deposition, the NO density decreases while that of NO_2 initially increases and then decreases. The decrease is attributable to a decrease in its rate of formation from reactions involving NO. The computed NO densities agree well with the experiments whereas agreement for the case of NO_2 is within 15–20%. Given the agreement with the NO density, the less good agreement for NO_2 is attributable to the disposition of N atoms from NO forming NO_2 and other N containing products, and the destruction of NO_2. For example, the density of the dominant N-containing products HNO_3, HNO_2, CH_3ONO_2 and CH_3ONO, are shown in figure 3(b). The rate coefficient for formation of the major product, HNO_3, has an uncertainty of ≈25% [29] and this uncertainty accounts for a large proportion of the disagreement.

The gas mixture discussed in the remainder of this article contains 8% O_2, 6% H_2O, 7% CO_2, 400 ppm CO, 260 ppm NO, 133 ppm H_2, 500 ppm propene (C_3H_6) and 175 ppm propane (C_3H_8) with the balance being N_2. This composition was chosen to assist comparison to experiments conducted at Ford Research Laboratories using a DBD device [30]. The processed gas in the experiments was analysed with a chemiluminescent NO_x analyser and a Fourier transform infrared (FTIR) spectrometer.

A baseline was obtained by performing simulations for a single pulse having a duration $\approx 10^{-7}$ s. The electron density (n_e) and temperature (T_e) as a function of time for the base case are shown in figure 4(a). The maximum electron density is $\approx 10^{13}$ cm^{-3} at which time $T_e \approx 3$ eV. When the voltage is switched off, electron densities decay due to dissociative attachment with H_2O (69%), O_2 (20%), CO_2 (3%), dissociative recombination with $H_3O^+ \cdot H_2O$ (2%) and non-dissociative attachment with O_2 (6%).

$$e + H_2O \rightarrow H^- + OH \quad (30)$$

$$e + O_2 \rightarrow O^- + O \quad (31)$$

$$e + CO_2 \rightarrow CO + O^- \quad (32)$$

$$e + H_3O^+ \cdot H_2O \rightarrow H + H_2O + H_2O \quad (33)$$

$$e + O_2 + M \rightarrow O_2^- + M. \quad (34)$$

O^-, H^- and O_2^- then neutralize with positive ions, dominated by $H_3O^+ \cdot H_2O$, to form neutral products,

$$O^- + H_3O^+ \cdot H_2O \rightarrow OH + H_2O + H_2O \quad k = 3.0 \times 10^{-6} \text{ cm}^3 \text{ s}^{-1} \quad (35)$$

$$H^- + H_3O^+ \cdot H_2O \rightarrow H_2 + H_2O + H_2O \quad k = 3.0 \times 10^{-6} \text{ cm}^3 \text{ s}^{-1} \quad (36)$$

$$O_2^- + H_3O^+ \cdot H_2O \rightarrow O_2 + H + H_2O + H_2O \quad k = 3.0 \times 10^{-6} \text{ cm}^3 \text{ s}^{-1}. \quad (37)$$

After approximately 3×10^{-7} s, ions have neutralized and recombined, and the chemistry is dominantly driven by neutral radicals, mostly OH, O, N and HO_2. The densities of OH, O, N and HO_2 are shown in figure 4(b) for the base case. O, N and OH are mainly generated by electron impact reactions

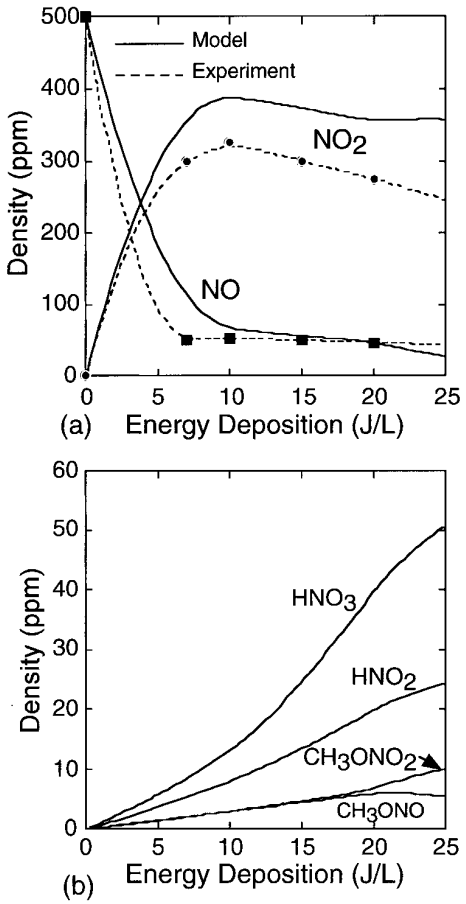

Figure 3. NO and NO_2 exit densities as a function of energy deposition. Feed gas is at 260 °C and contains 500 ppm NO, 500 ppm C_3H_6, 10% O_2, 10% H_2O and balance N_2: (a) Experiment [28] and model results; (b) exit densities of major N containing products.

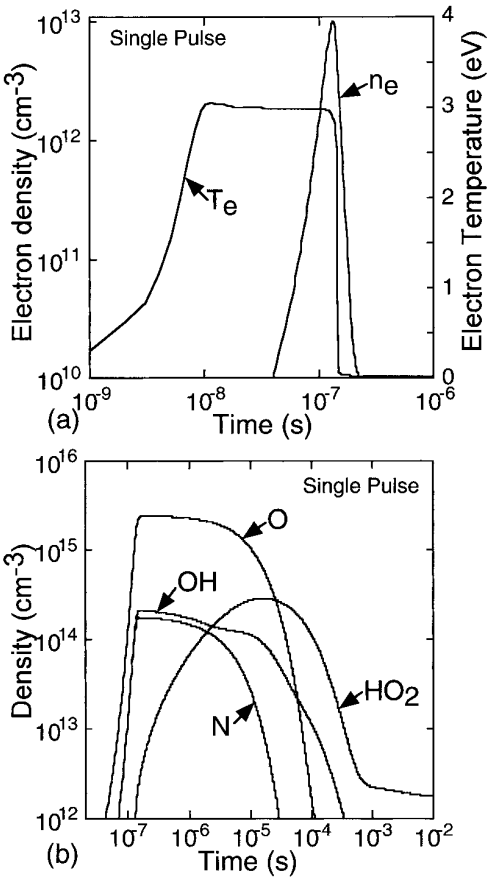

Figure 4. Plasma properties during the single-pulse discharge processing of NO_x: (a) n_e and T_e; (b) O, OH, N and HO_2. The background gas mixture is the same as in figure 1 with 500 ppm C_3H_6 and 175 ppm C_3H_8.

(equations (4)–(6)). HO_2 is mainly produced as an end product of the NO–R–OO radical reactions (67%), by the reaction of H with O_2 (11%) (equation (8)) and by the reaction of HCO with O_2 (22%),

$$\mathrm{HCO} + \mathrm{O_2} \rightarrow \mathrm{HO_2} + \mathrm{CO}$$
$$k = 2.0 \times 10^{-14}(T/298)^{2.38} \exp(768/T)\ \mathrm{cm^3\ s^{-1}},$$
$$k_{298} = 2.6 \times 10^{-13}\ \mathrm{cm^3\ s^{-1}}. \qquad (38)$$

NO is dominantly consumed by conversion to NO_2 by reactions with O, O_3, HO_2, and R–OO in proportions of 2%, 1%, 38% and 45% (equations (2) and (21)). Some amount of NO remediation also occurs by the reaction with OH to form HNO_2 (2%) (equation (2*d*)) and by the formation of organic nitrites (8%) (equations (24) and (28)).

To investigate multiple pulse excitation, 20 pulses were applied over the residence time of 0.2 s at 100 Hz while keeping the total energy deposition constant. The electron density and temperature, during the first pulse and the last pulse for the base case are shown in figure 5. The lower energy deposition/pulse was obtained by decreasing the voltage. The electron density reaches a maximum of 5×10^{11} cm^{-3} at which time T_e peaks to 3 eV. The current pulses are longer compared to the single-pulse case in spite of the lower peak electron density because of the longer time required to avalanche due to the lower applied voltage. The lower energy deposition per pulse results in a peak electron density approximately 3% that of the single pulse, which is less than 1/20 of the single pulse due to the lower ionization efficiency at lower voltage. The electron temperature does not significantly change since multistep excitation is not important for these conditions and so the ionization source is dominated by electron impact with ground state species. The electron density and the temperature for the 20th pulse are essentially the same as for the first pulse because of the almost constant composition of the background gas mixture.

The densities of O, N, OH and HO_2 during the first pulse are shown in figure 6(a) and for the 20th pulse in figure 6(b). The maximum densities of O, N, OH and HO_2 are ≈4.6% that of the single pulse because of the lower energy deposition and lower excitation efficiency of the lower voltage. The maximum O, N and OH densities are nearly unchanged for each of the 20 pulses since the density of the feedstock gases for the generation of O, N and OH, O_2, N_2 and H_2O do not change significantly. The rate of decay of O is essentially the same for the first and the 20th pulse whereas the rate of decay of N is slower for the 20th pulse because the density of NO, the main consumer of N atoms, has decreased by that time, as shown in figure 7. The decay of OH is more rapid during the 20th pulse compared to the first pulse because of the increased rate of reaction of OH with NO_2 (equation (3)), which has a

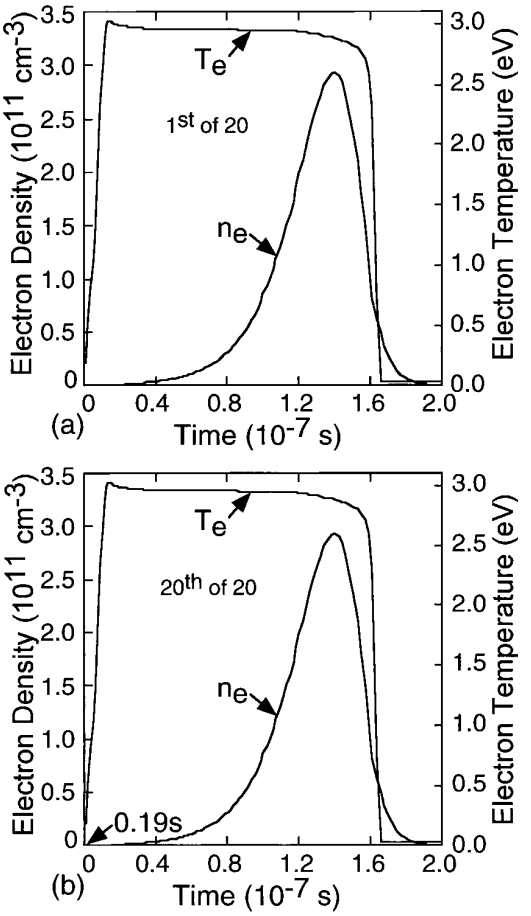

Figure 5. Electron density and temperature during the multiple pulse discharge processing of NO_x: (a) first of 20 pulses; (b) 20th of 20 pulses. Electron densities and temperature are almost the same for all the pulses because the background gas mixture does not significantly change during the previous pulses. The gas mixture is the same as in figure 4.

higher density by the 20th pulse. The rate of decay of HO_2 is significantly smaller for the 20th pulse because the density of NO, which is the main consumer of HO_2, has decreased significantly. Unresolved HO_2 radical densities are shown in figure 6(c). As the NO density decreases with each pulse, the density of HO_2 increases as its rate of consumption with NO decreases (equation (2*c*)).

The densities of NO and NO_2 for single- and multiple-pulse excitation are compared in figure 7. With a single pulse, the NO density decreases from 4.2×10^{15} to 1.0×10^{14} cm^{-3} at $t = 0.2$ s resulting in approximately 98% NO remediation. With multiple pulses, the exit densities of NO are higher than with a single pulse. This is due to the regeneration of NO from NO_2 by,

$$NO_2 + O \rightarrow NO + O_2$$
$$k = 6.5 \times 10^{-12} \exp(120/T) \text{ cm}^3 \text{ s}^{-1},$$
$$k_{298} = 9.7 \times 10^{-12} \text{ cm}^3 \text{ s}^{-1}. \quad (39)$$

CH_3O is a transient species as shown in figure 8. It is generated by the reaction of CH_3O_2 with NO (equation (23)), and consumed by reactions with NO and NO_2 (equations (24) and (25)) to produce CH_3ONO and CH_3ONO_2, respectively. The reaction rate coefficients for these processes are

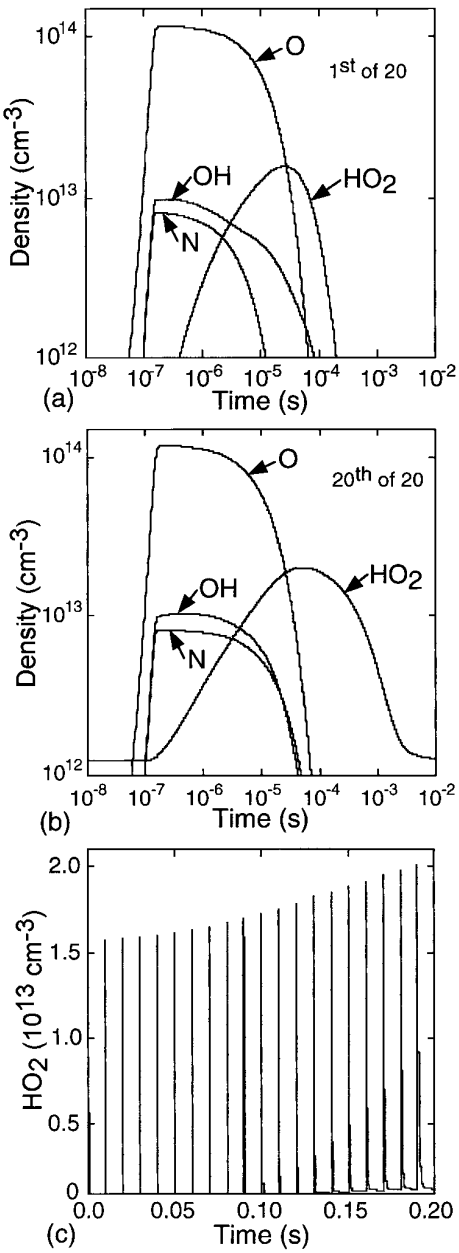

Figure 6. Molecular and radical densities during the multiple pulse plasma processing of NO_x: (a) O, OH, HO_2 and N during the first pulse; (b) O, OH, HO_2 and N for the 20th pulse; (c) unresolved HO_2 densities during the full length of the residence time. Peak HO_2 densities increase with time owing to the lower rates of reaction with NO, the main consumer of HO_2. Conditions are the same as in figure 4.

approximately the same and so their relative rates are determined by the relative concentrations of NO and NO_2. With a single pulse, the density of NO greatly exceeds NO_2 when the density of CH_3O is maximum. Hence, most of the CH_3O is lost in the reaction with NO forming CH_3ONO and the production of CH_3ONO_2 is low. With multiple pulses, CH_3O is produced during each pulse. With each successive pulse, the concentration of NO decreases and that of NO_2 increases. When the concentration of NO_2 exceeds that of NO, CH_3O is consumed preferentially by NO_2 forming CH_3ONO_2 as opposed to reacting with NO. This leads to an

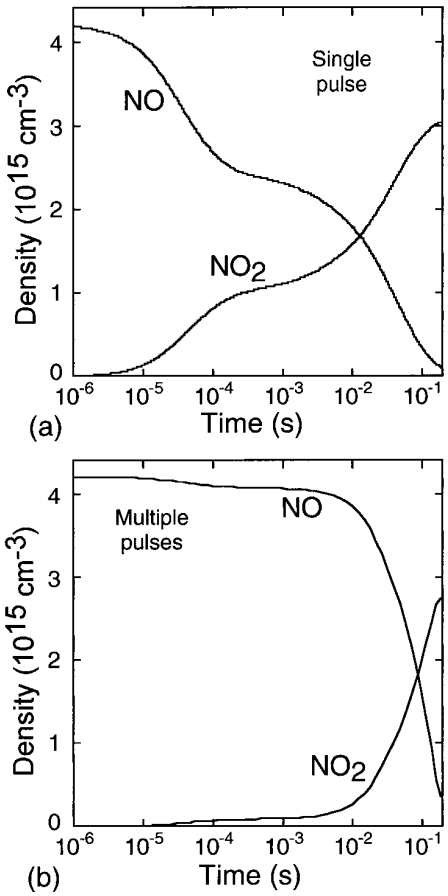

Figure 7. Comparison of NO, and NO_2 densities during the single and multiple discharge processing of NO_x. Conditions are the same as in figure 4: (a) Single pulse; (b) multiple pulses.

increase in NO_x remediation since CH_3ONO_2 is a terminal product.

With a single pulse, NO remediation is almost 98%, whereas with multiple pulses, the exit densities of NO are higher due to the regeneration from NO_2 through the reaction in equation (39). With a single pulse, the density of O decays before the density of NO_2 increases to a significant level. As a result, the regeneration process is not important. For later pulses, the densities of O and NO_2 are high at the same time, resulting in NO_2 reduction and formation of NO. This trend is shown in figure 9. During the initial pulses, NO is mainly converted to NO_2 ($t < 0.05$ s) and the density of NO_2 increases. At later times, as the concentration of NO_2 increases, NO and NO_2 come into a pulse-to-pulse equilibrium. After approximately 0.05 s, at the start of each pulse, NO_2 is converted to NO by the reaction with O atoms (equation (39)) and at later times during the same pulse, the NO is converted back into NO_2 (equations (2) and (21)).

The densities of CH_3ONO_2 for single- and multiple-pulse formats for an energy deposition of 70 J L^{-1} are shown in figure 10. The final concentration with multiple pulses is ≈2.5 times that produced with a single pulse. This difference is due to the increased temporal overlap of CH_3O and NO_2 in the multiple-pulse case in comparison with the single pulse.

The exit densities of NO as a function of energy deposition are shown in figure 11(a). For energy depositions >40 J L^{-1},

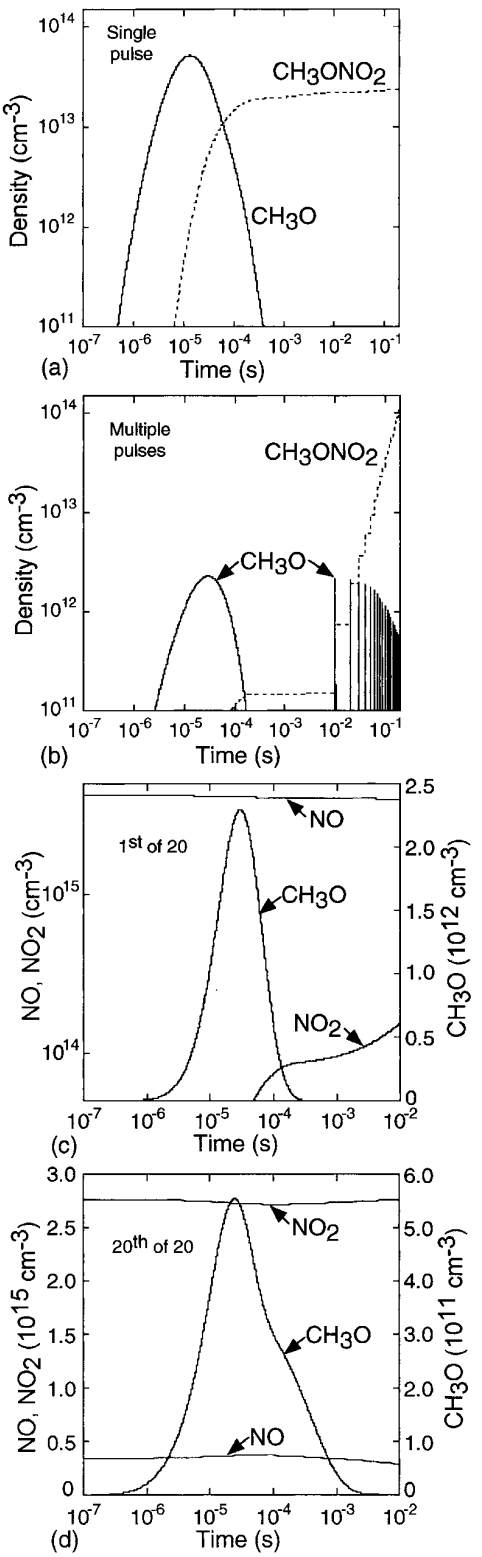

Figure 8. CH_3O, CH_3ONO_2, NO and NO_2 densities for single- and multiple-pulse discharge processing of NO_x. Conditions are the same as in figure 4. CH_3O and CH_3ONO_2 densities for (a) single pulse; (b) multiple pulses. NO, NO_2 and CH_3O densities for (c) the first of 20 pulses; (d) the 20th of 20 pulses. With multiple pulses, NO densities are gradually lowered and NO_2 densities are gradually increased. CH_3O is produced during each pulse. When $[NO_2] > [NO]$, the formation of CH_3ONO_2 commences. CH_3O density decreases with each pulse, because the source of CH_3O, C_3H_6, decreases with each pulse.

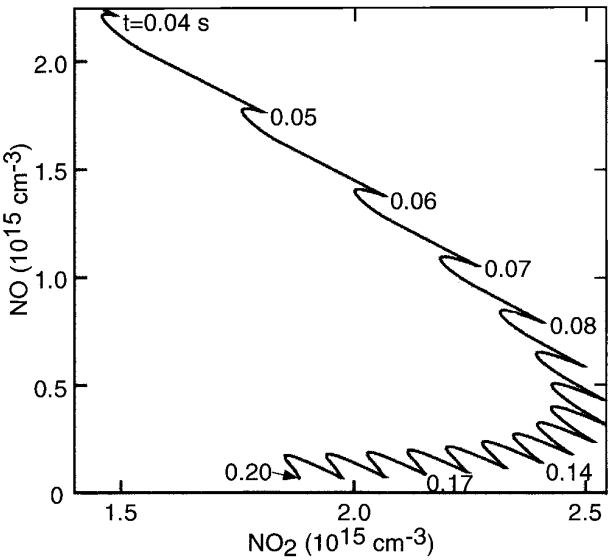

Figure 9. Variation of NO with NO_2. The curve corresponds to a time evolution. At $t < 0.05$ s, $NO + O \rightarrow NO_2$ dominates over $NO_2 + O \rightarrow NO + O_2$ due to the smaller density of NO_2. As a result, in each of the pulse periods after 0.05 s, there is an initial back conversion of NO_2 to NO and a later conversion of NO to NO_2. The contribution to NO formation from the initial back conversion of NO_2 becomes larger as the concentration of NO_2 increases.

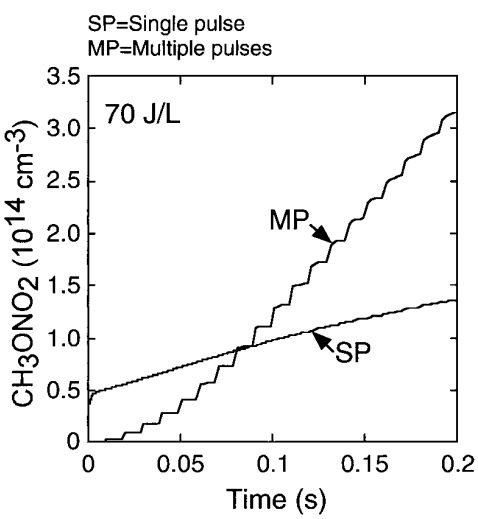

Figure 10. CH_3ONO_2 density as a function of time for single- and multiple-pulse formats. The energy deposition is 70 J L^{-1} and other conditions are the same as in figure 4.

almost 100% of the NO is removed with a single pulse, a major fraction of (∼65%) which reappears as NO_2. With increasing energy deposition, a larger fraction of this NO_2 is converted to HNO_3. With multiple pulses, NO conversion is lower compared to the single-pulse case due to the regeneration of NO from NO_2 (equation (39)). The exit NO densities obtained using multiple pulses agree more closely with experimental results than with single pulses. The efficiency of these processes can be quantified by W-values. (W-value [eV/molecule] is the amount of energy required to remove one molecule of the compound. Lower values correspond to more efficient processes.) The W-values for NO_x as a function of energy deposition are also shown in figure 11(a).

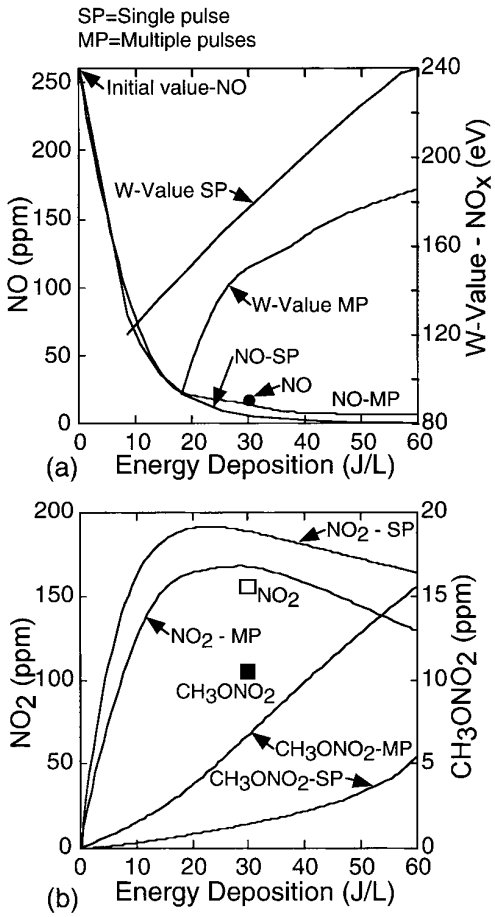

Figure 11. Effect of energy deposition on NO_x remediation: (a) NO and W-value for NO_x; (b) NO_2 and CH_3ONO_2. Experimental values for NO (●), NO_2 (□) and CH_3ONO_2 (■) are also shown. In general, the W-values for multiple-discharge formats are lower, indicating higher efficiencies of remediation. NO_2 densities for multiple discharge formats are lower because of the back conversion to NO ($NO_2 + O \rightarrow NO + O_2$). The differences in CH_3ONO_2 between single- and multiple-pulse formats increases with energy deposition because of the increased production of CH_3O and NO_2.

The W-values for NO_x are lower (more efficient) with multiple pulses. At low-energy deposition (≈20 J L^{-1}), W-values are ≈110 eV for multiple pulses compared to 153 eV for a single pulse. At high-energy deposition (≈60 J L^{-1}), W-values for multiple pulses are ≈185 eV compared to 240 eV for a single pulse. The decrease in the W-values is a result of the additional removal of NO_x through the formation of larger amounts of HNO_2, HNO_3 and CH_3ONO_2.

The densities of NO_2 and CH_3ONO_2 as a function of energy deposition with single and multiple pulses are shown in figure 11(b). As before, the values obtained using multiple pulses agree more closely with the experimental results. With multiple pulses, more NO_2 is channelled into reactions with OH, CH_3O and O (equations (3), (25) and (39)) because, with each pulse, NO_2 is present when O, OH and CH_3O have large densities. As a result, the NO_2 densities are lower. With increasing energy deposition, the exit concentrations of NO_2 initially increase and then decrease. The decrease is due to the increased production of O, OH and CH_3O at higher energy deposition, which then consume NO_2 to produce NO, HNO_3 and

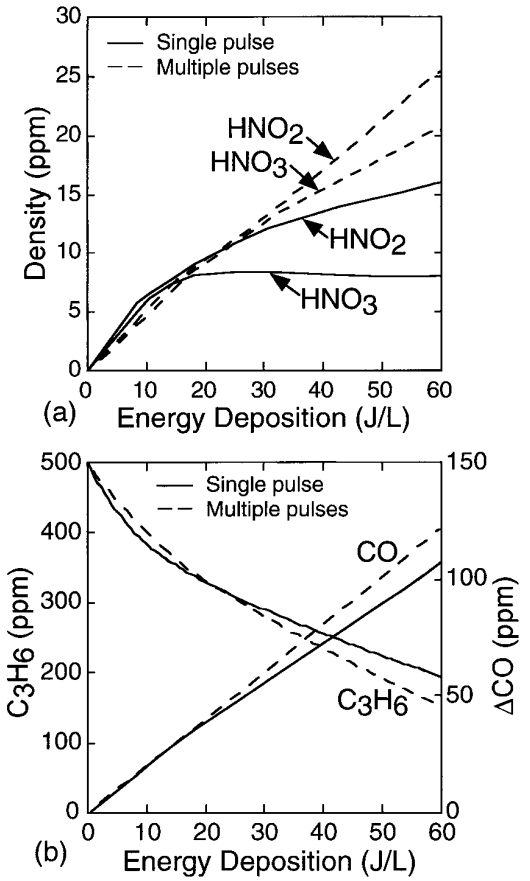

Figure 12. Exit UHC and end-product densities as a function of energy deposition: (a) HNO_2 and HNO_3; (b) C_3H_6 and CO. Single-pulse (full curves) and multiple-pulse (dashed curves) formats. HNO_x densities are higher with multiple-pulse formats due to the increased production from NO_2. Higher C_3H_6 conversion is observed with multiple-pulse formats due to the increased production of OH from HO_2 ($HO_2 + NO \rightarrow NO_2 + OH$). CO production increases with multiple-pulse formats due to the increase in the production of HCO from HCHO ($HCHO + OH \rightarrow HCO + H_2O$; $HCO + O_2 \rightarrow CO + HO_2$).

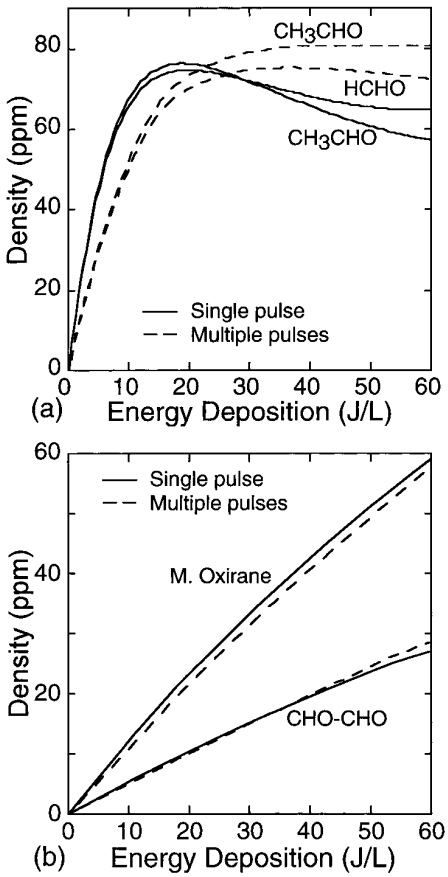

Figure 13. Exit hydrocarbon end product densities as a function of energy deposition: (a) HCHO, CH_3CHO; (b) methyl oxirane, CHO–CHO. Single-pulse (full curves) and multiple-pulse (dashed curves) formats.

CH_3ONO_2, respectively. The difference in CH_3ONO_2 densities between single- and multiple-pulse formats increases with increasing energy deposition. This is because, at high-energy deposition, larger quantities of CH_3O and NO_2 are produced which results in more CH_3ONO_2 when their peak densities coincide.

The exit densities of N-containing products, HNO_2 and HNO_3, as a function of energy deposition are shown in figure 12(a). The densities with multiple pulses are generally higher. HNO_2 is produced by the reaction of OH with NO (equation (2*d*)). The higher HNO_2 density with multiple pulses is due to the increase in the rate of the reaction,

$$HO_2 + NO_2 \rightarrow HNO_2 + O_2 \qquad k = 1.2 \times 10^{-13}\ \text{cm}^3\ \text{s}^{-1}. \tag{40}$$

Since the concentration of NO_2 increases with each pulse, high densities of HO_2 and NO_2 can coincide, a condition which does not significantly occur with a single pulse. As a result, the contribution from this reaction to HNO_2 production also increases. HNO_3 is produced by the reaction of NO_2 and OH (equation (3)). With the increase in NO_2, the HNO_3 density also increases as OH and NO_2 also have high densities at the same time with multiple pulses.

The consumption of C_3H_6 as a function of energy deposition is shown in figure 12(b). At higher energy deposition, C_3H_6 consumption is higher with multiple pulses due to the increased production of OH by the reaction of HO_2 with NO (equation (2*c*)). HCO production also increases with multiple pulses due to the reaction of OH with the increasing density of HCHO,

$$OH + HCHO \rightarrow HCO + H_2O$$
$$k = 4.73 \times 10^{-12}(T/298)^{1.18} \exp(225/T)\ \text{cm}^3\ \text{s}^{-1},$$
$$k_{298} = 1.0 \times 10^{-11}\ \text{cm}^3\ \text{s}^{-1}. \tag{41}$$

The production of CO therefore also increases with multiple pulses due to the increase in the production of HCO radicals, which then react with O_2 to produce CO (equation (38)).

The final C-containing products HCHO, CH_3CHO, methyl oxirane and CHO–CHO are shown in figure 13. HCHO and CH_3CHO are generated as the end-products of the OH-initiated reactions with C_3H_6. With multiple pulses, the NO density is higher (because of the $NO_2 \rightarrow NO$ conversion) which results in higher rates of reactions with peroxy radicals (equation (21)). This increases the production of HCHO and CH_3CHO. The pathway leading to the production of HCHO and CH_3CHO is described in detail in [26]. Briefly, the product RO of the reaction of peroxy radicals with NO (equation (21))

decomposes to produce HCHO, CH_3CHO and hydroxyalkyl radicals. These hydroxyalkyl radicals further react with O_2 to produce HO_2 and more HCHO, and CH_3CHO. Methyl oxirane and CHO–CHO are products of the O atom initiated reactions with C_3H_6. Only small differences are observed in the densities of these species between single and multiple pulses because the initiating species, O, is not significantly affected by multiple pulses.

5. Concluding remarks

The consequences of multiple discharge pulses on the plasma remediation of NO_x in the presence of hydrocarbons was numerically investigated. When using multiple pulses, reactions occur in the latter pulses with reaction products from previous pulses which are not accessible with a single pulse. For example, less than 1 ppm of CH_3ONO_2 was formed with a single pulse whereas nearly 10 ppm was produced when the same energy was distributed over 20 pulses. Comparison of the products of single- and multiple-pulse discharges showed marked differences in final concentrations of NO_2, HNO_x, C_3H_6 and CO. W-values for NO_x decreased from 240 eV for a single pulse to 185 eV when the same energy was distributed over 20 pulses.

Acknowledgments

The authors would like to thank John Hoard of the Ford Motor Company and J M Pouvesle from the University of Orleans, France, for providing experimental data. This work was supported by Ford Motor Company and the National Science Foundation (CTS 99-74962).

References

[1] Person J C and Ham D O 1988 *Radiat. Phys. Chem.* **31** 1
[2] Helfritch D J 1993 *Non-Thermal Plasma Techniques for Pollution Control-Part B: Electron Beam and Electrical Discharge Processing* ed B M Penetrante and S Schulthesis (New York: Springer) p 33
[3] Frank N W 1995 *Radiat. Phys. Chem.* **45** 989
[4] Frank N W, Hirano S and Kawamura K 1988 *Radiat. Phys. Chem.* **31** 57
[5] Frank N W, Kawamura K and Miller G 1985 *Radiat. Phys. Chem.* **25** 35
[6] Fuchs P, Roth B, Schwing U, Angele H and Gottstein J 1988 *Radiat. Phys. Chem.* **31** 45
[7] Helfritch D J and Feldman P 1984 *Radiat. Phys. Chem.* **24** 129
[8] Jordan S 1988 *Radiat. Phys. Chem.* **31** 21
[9] Penetrante B M, Hsiao M C, Merritt B T, Vogtlin G E, Wallman P H, Neiger M, Wolf O, Hammer T and Broer S 1996 *Appl. Phys. Lett.* **68** 3719
[10] Penetrante B M, Hsiao M C and Merritt B T 1995 *Trans. Plasma Sci.* **23** 679
[11] Park J Y, Toicic I, Round F G and Chang J S 1999 *J. Phys. D: Appl. Phys.* **32** 1006
[12] Naidis G 1997 *J. Phys. D: Appl. Phys.* **30** 1214
[13] Tas M, van Hardeveld R and van Veldhuizen E 1997 *Plasma Chem. Plasma Process.* **17** 371
[14] van Veldhuizen E, Rutgers W and Bityurin V 1996 *Plasma Chem. Plasma Process.* **16** 227
[15] Mok Y S, Ham S W and Nam I 1998 *Trans. Plasma Sci.* **26** 1566
[16] Niessen W, Wolf O, Schruft R and Neiger M 1998 *J. Phys. D: Appl. Phys.* **31** 542
[17] McLarnon C R and Penetrante B M 1998 S.A.E. 982434
[18] McLarnon C R and Penetrante B M 1998 S.A.E. 982433
[19] Gentile A C and Kushner M J 1995 *J. Appl. Phys.* **78** 2074
[20] Takaki K, Jani M A and Fujiwara T 1999 *Trans. Plasma Sci.* **27** 1137
[21] Sun W, Pashaie B, Dhali S and Honea F 1996 *J. Appl. Phys.* **79** 3438
[22] Penetrante B M, Brusasco R M, Merritt B T, Pitz W J, Vogtlin G E, Kung M C, Kung H H, Wan C Z and Voss K E 1998 S.A.E. 982508
[23] Balmer M L, Tonkyn R, Yoon S, Kolwaite A, Barlow S, Maupin G, Orlando T and Hoard J 1999 S.A.E. 1999-01-3640
[24] Dorai R and Kushner M J 1999 S.A.E. 1999-01-3683
[25] Vitello P, Penetrante B M and Bardsley J 1994 *Phys. Rev.* E **49** 5575
[26] Dorai R 2000 *MS Thesis* University of Illinois <http://uigelz.ece.uiuc.edu>
[27] Hindmarsh A 1987 *Livermore Solver for Ordinary Differential Equations* (Lawrence Livermore Laboratories)
[28] Khacef A, Nikravech M, Motret O, Lefaucheux P, Viladrosa R, Pouvesle J M and Cormier J M 2000 Private communications
[29] Fulle D, Hamann H F, Hippler H and Troe J 1998 *J. Chem. Phys.* **108** 5391
[30] Hoard J 2000 Private communications